

Synthesis and characterization of polyacrylonitrile based precursor beads for the removal of the dye malachite green from its aqueous solutions

Ola Abd Al-Qader Mahmood, Basma I. Waisi*

Department of Chemical Engineering, College of Engineering, University of Baghdad, Baghdad, Iraq,
emails: basmawaisi@coeng.uobaghdad.edu.iq (B.I. Waisi), olaabdalqader25@gmail.com (O. Abd Al-Qader Mahmood)

Received 11 July 2020; Accepted 7 December 2020

ABSTRACT

Polyacrylonitrile (PAN) precursor beads-shape with uniform particle size was prepared by phase inversion method and used for dye removal from aqueous solution. The morphology, diffraction patterns, pore size distribution, and chemical structure of the prepared PAN precursor beads were confirmed by scanning electron microscopy, X-ray diffraction analysis, physisorption analyzer, and Fourier-transform infrared spectroscopy, respectively. The structure of the prepared PAN precursor beads contains a porous structure with many large finger-like defects. The pores on the surface appear to be linked to those inside the bead. Malachite green (MG) dye was used as a model contaminant to investigate the prepared PAN precursor beads' adsorption capacity. The effect of different adsorption parameters, such as initial dye concentration, adsorbent dosage, pH of the solution, rotational speed, and temperature, were investigated. The effective pH was 7 and the process reached equilibrium in 5 h. Maximum dye elimination was 97% under optimal conditions: PAN dosage was 0.4 g, rotational speed was 200 rpm, initial concentration was 10 mg/L, and the temperature was 15°C. The adsorbent was regenerated and reused for MG dye adsorption showing a good removal up to 81% after the fifth run. The Langmuir and Freundlich adsorption models were used to characterize the equilibrium isotherms, and the former was ideally suited. Kinetic analysis showed that MG dye adsorption on PAN precursor bead followed a pseudo-second-order. The thermodynamic study has demonstrated that adsorption is a spontaneous and endothermic process.

Keywords: Adsorption; Malachite green; Polymer; Beads; Isotherm; Kinetic; Thermodynamic

1. Introduction

Industrial wastewater contains many organic and inorganic contaminants that have to be purified before being discharged to the environment, including dyes. Dyes present in the effluents of various industries such as textile, wool, leather, silk, papers, pulps, inks, cosmetics, pharmaceutical, and food industries [1,2]. Over the last decade, industrial growth has contributed to the rise of dye production; approximately 7×10^5 ton/y are used worldwide, where the textile industry consumes 2/3 of the dyes [3]. The main problem with dyes is the large number and quantity

and the chemical structure of some dyes, making them stable and non-biodegradable [4]. Some dyes, including malachite green (MG), are hazardous and detrimental even at low concentrations; it harms the aquatic organisms by changing the color of the water, consequently reducing the penetration of the light and reducing the photosynthesis of aquatic plants [5]. MG which is known as Aniline green, or diamond green, is a green crystal cationic dye soluble in water with the chemical formula ($C_{23}H_{26}N_2Cl$) as shown in Fig. 1 [6]. The MG dye is mainly used in the coloring of cotton, wool, paper, leather, and acrylic industries [6–8]. It is also used as a pH indicator due to its color changes from

* Corresponding author.

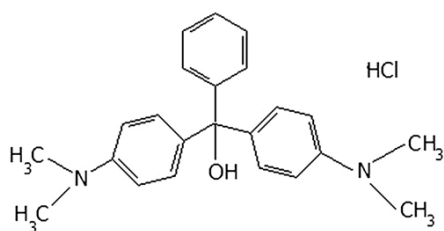


Fig. 1. Malachite green (MG) dye structure [6].

yellow (at low pH) to green (at high pH) [9]. Although MG dye is prohibited by the US Food and Drug Administration for application in animals used for human consumption, it is still being used in some countries due to its low cost and availability [5]. MG effluent is harmful that can cause eye and skin irritation, nausea, and diarrhea. Also, respiratory issues arise as the effluent contaminants are inhaled when they evaporate [9]. It can also irritate and harm the immune and nervous systems of marine creatures [10,11].

Various methods have been used to remove dyes before discharging, including physicochemical and biological processes such as membrane filtration [12], photocatalytic [13,14], biodegradation [15,16], and adsorption [17,18]. Adsorption is one of the most promising and effective techniques for contaminants removal from wastewater, including dyes, due to the ease of the process, high reliability, and applicability for large-scale wastewater treatment [19,20]. Adsorbents are of strong technical importance due to their possibilities to bind with particular pollutants, as well as achieving a high degree of purification, especially of wastewaters with low pollutant concentrations because of their characteristics, including a wide variety of complex surfaces, special pores, and tunable pores surface properties [21–23].

Various porous materials, including carbon-based nano-adsorbents, have been demonstrated as efficient adsorbents for dye removal in terms of either adsorption capacity or adsorption kinetics. However, attributable to the high costs of activation and regeneration, researchers are continuously searching for developing cost-effective adsorbents [24]. MG dye was removed from water using various materials, including wood apple shell [25], saklikent mud [26], bio-polymer [27], and polyaniline-*Alstonia scholaris* leaves composite [9]. Also, polymeric adsorbents were used to remove MG dyes such as cyclodextrin polymer powder [28], imprinted polymers [29], and poly(styrene-co-acrylonitrile) nanofiber [30].

To achieve high MG dye adsorption performance, adsorbent materials must have favorable physicochemical characteristics that depend on the raw materials' properties and the preparation parameters [31]. The mesoporous structure is also a critical characterization of the adsorbent to enhance the adsorption capacity. Although powder-type adsorbent has high adsorption capacity due to its high surface area and short diffusion distance to the adsorption site, fine powder causes a significant pressure drop leading to an operational problem in the adsorption system. Thus, in adsorbent columns, shaped adsorbent materials (such as beads) are preferred because they can be easily separated and handled [32].

This work deals for the first time with preparing polyacrylonitrile based precursor beads adsorbent for effective removal of MG dye from aqueous water. Polyacrylonitrile (PAN) precursor beads were synthesized by the phase inversion method using polyacrylonitrile polymer as a precursor. The synthesized PAN precursor beads have a uniform particle size of 3 mm with a well-developed mesoporosity. The effects of dye's initial concentration, adsorbent dosage, pH of the solution, rotation speed, and temperature have been studied. Kinetic, isothermal, thermodynamic properties, and adsorbent regeneration have also been investigated. The MG dye reduction was based on Langmuir isotherm and pseudo-second-order kinetic analysis. The thermodynamic properties showed a spontaneous and endothermic adsorption mechanism.

2. Materials and methods

2.1. Materials

Malachite green hydrochloride dye (MG) ($(C_{23}H_{26}N_2Cl)$, M.wt 346 g/mol) was purchased from Sigma-Aldrich, USA. Polyacrylonitrile (PAN) ($(C_3H_3N)_n$, M.wt_{avg.} 150,000 g/mol) was purchased from Macklin, China. Dimethylformamide (DMF) was ordered from Solvochem, UK. All chemicals were used without any further purification. HCL and NaOH from Sigma-Aldrich, USA. (1 M) were used for adjusting the pH of the adsorbate solution.

2.2. Precursor beads synthesis

A specific amount of PAN was dissolved in DMF to prepare 16 wt.%PAN/DMF solutions under continuous stirring in a water bath at 60°C until a homogeneous light yellow mixture has been obtained. After the mixture was rested to allow air bubbles to escape, it was placed in a 10 ml plastic syringe and dropped into a coagulation bath. Distilled hot water at 80°C was used as the external coagulant medium. When the polymeric solution (PAN/DMF) contacted the coagulant medium (hot water), spherical precipitates were formed. The precursor beads were left in DI water for 2 d to remove the residual solvent, and the phase inversion complete. Finally, it was left to be dried at room temperature for 2–3 d, and the result was 3 mm size of soft white color bead-shape as shown in Fig. 2.

2.3. Precursor beads characterization

Scanning electron microscopy (SEM) images of PAN precursor beads samples were characterized using field emission scanning electron microscopy (FESEM, JEOL 6335F) to determine the surface and cross-section morphologies. The crystalline characteristics of the samples were examined by X-ray diffraction (XRD) (model: DY5238 ID 205521) instrument with 2θ range from 0° to 80° and scan rate 2 (°/min) using Cu-K α as a radiation source. Nitrogen adsorption/desorption isotherms of PAN prepared beads were obtained from the Physisorption Analyzer (Micromeritics Instrument Corporation). The samples were first degassed at 150°C for 2 h and then analyzed for nitrogen sorption at 77 K. The specific surface area was determined



Fig. 2. Digital photo image of PAN-based precursor beads.

by applying the Brunauer–Emmett–Teller (BET) formula while the total pore volume and pore size distribution were calculated by the Barret–Joyner–Halenda (BJH) method. The Fourier-transform infrared spectroscopy (FTIR) test was conducted using a Nicolet iS10 FTIR (Thermo Scientific) to clarify PAN prepared beads' surface chemistry. In addition, the point zero charge (pH_{pzc}) that represents the adsorbent surface was determined, as mentioned by others [33]. NaCl (0.1 M) was prepared and adjusted at different pH values ranging from (2–9). A 50 mL of the solution was placed in a closed Erlenmeyer flask, and 0.15 g of PAN-based beads precursor was added. Then the samples were agitated at room temperature at 200 rpm for 48 h. The point zero charges (pH_{pzc}) is the point where the final pH – initial pH = 0.

2.4. Batch study

A stock solution of 1,000 mg/L MG dye was prepared by dissolving a sufficient MG quantity in a specific distilled water volume. The desired concentrations of adsorbate were prepared by diluting the stock solution with distilled water. The pH value was measured using the pH meter ((pH-200) model). Dye concentrations were measured using a UV/Vis spectrophotometer (Thermo Scientific Genesys 10S) at a wavelength of 618 nm [2].

The equilibrium batch study was employed to investigate the impact of the initial dye concentration, pH of the solution, adsorbent amount, rotational speed, and temperature. All batch experiments (except those to evaluate the variables) were carried out using 50 mL of 10 mg/L dye and 0.4 g beads at room temperature (15°C) and neutral pH. All the samples were placed in a shaker (Karl Kolb, Germany) at a constant oscillation of 200 rpm. The pH of the solution varies (3–10) to find the most effective pH value for; removing MG, diluted HCl, or NaOH was used to adjust the pH of the solution. The dose of PAN precursor beads (0.2–1) g was used to evaluate the adsorbent effect. Different initial concentrations of the dye (5–25) mg/L were

used to indicate the adsorbate effect. The speed of rotation in the range of (100–300) rpm was used to detect the mixing rate effect. Control experiments (without the use of adsorbent) were conducted to ensure that the glass of beakers did not induce the reduced concentration of dye.

The samples were extracted from the solutions at various intervals (15, 30, 45, and 60) min then every hour until equilibrium was reached. Dye concentration was measured before and after adsorption using a UV-VIS spectrophotometer. Each experiment was repeated three times, and an average value was used in the calculations.

3. Results and discussion

3.1. Precursor beads characterization

The SEM images of the surface and cross-section morphologies of PAN-based precursor beads are displayed in Fig. 3. It is obvious in Fig. 3a that the surface is rough with spacing ridge-and-valley morphology. The pores are not obvious on the surface shell due to the rough morphology of the surface. However, the cross-section image in Fig. 3b clearly shows a uniform and highly porous inner-surface structure inside the beads. As one moves away from the surface, the structure comprises porous morphology with several large finger-like holes, as shown in Fig. 3c. The pores on the surface seem to be interconnected with those in the inner part of the bead. This morphological feature can be explained by the precipitation mechanism dominated by instantaneous liquid–liquid demixing induced by the external coagulation medium [34].

XRD reflects the diffraction pattern of precursor PAN-based beads. As shown in Fig. 4, the XRD patterns have a main diffraction peak at around $2\theta = 17^\circ$, which is corresponding to the plane (100) of a hexagonal structure (related to $\text{C}\equiv\text{N}$) [35]. Another peak is around $2\theta = 25.2^\circ$ that is corresponding to ladder polymer (which is related to the $\text{C}=\text{N}$ group). It is fitting to the characteristic cyclization and aromatization structures of the (0 0 2) planes [36].

The specific surface area and the pore volume of PAN precursor beads were determined by the N_2 adsorption/desorption method. Fig. 5a shows a steep increase of N_2 adsorption capacity as the relative pressure (P/P_0) increased demonstrating type II adsorption isotherm according to the IUPAC classification. Fig. 5b shows PAN precursor beads samples displayed noticeable peaks in the range of 1–20 nm, which mainly indicates a mixture of microporous and mesoporous structure PAN-based precursor beads. Based on the above characterization results, PAN-based precursor beads were successfully synthesized using the phase inversion method. The PAN precursor beads' pore volume and BET surface area were found to be 0.07 cm^3/g , and 25 m^2/g , respectively.

The infrared spectra (FTIR) depicted in Figs. 6a and b show the functional groups on the solid surface of the prepared PAN precursor beads before and after MG dye adsorption, respectively. The observed peaks on the surface chemistry of the clean PAN beads at 1,062.7; 1,234.4; 1,737.8 and 2,241.2 cm^{-1} are assigned for $-\text{COOH}$ group, O–H bending, stretching $\text{C}=\text{O}$ group and stretching $\text{C}\equiv\text{N}$ band [37–39]. The peak at 2,930 and 3,650 cm^{-1} are due to

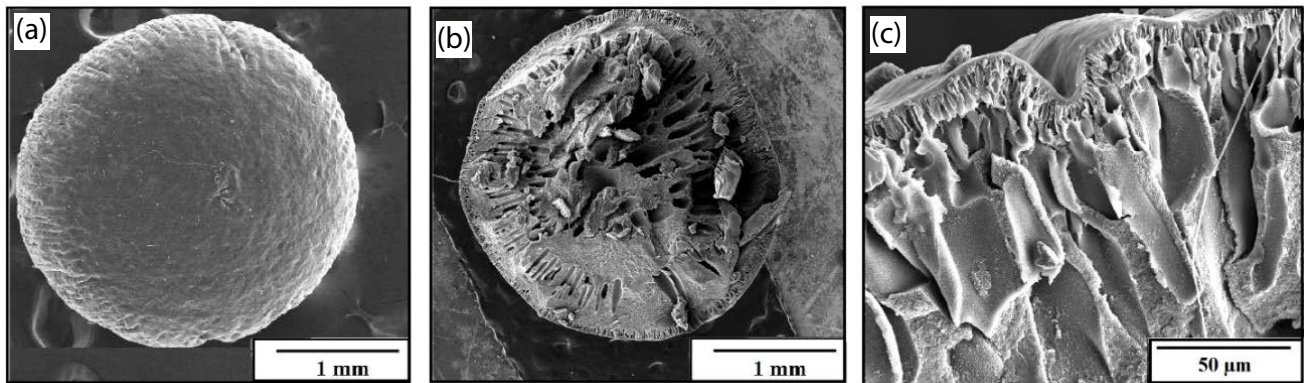


Fig. 3. SEM images of PAN-based precursor beads (a) surface morphology (magnification is 50 X), (b) cross-section (magnification is 50 X), and (c) high magnification (1,000 X).

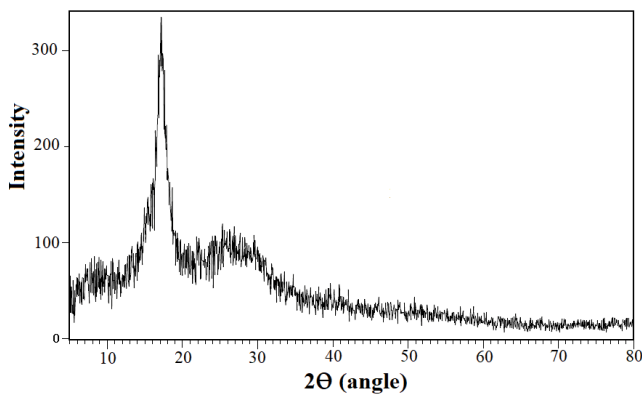


Fig. 4. XRD spectra of PAN-based precursor beads.

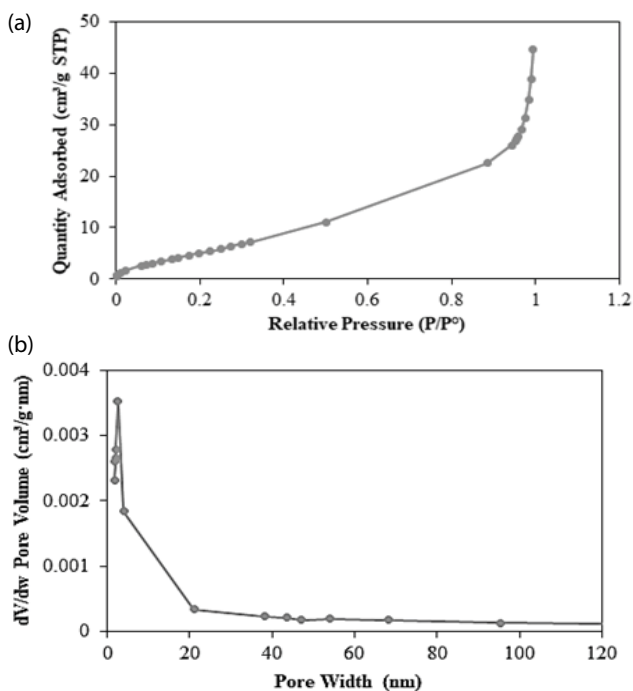


Fig. 5. (a) Nitrogen adsorption/desorption isotherm and (b) pore size distribution of PAN-based precursor beads.

aliphatic C–H stretching and free hydroxyl group [40,41]. Other peaks were observed in 1,370 and 1,450.4 cm^{-1} are aliphatic-CH group [42]. After MG dye adsorption on the PAN beads, most of the surface functional groups in the adsorbent were vanished or decreased due to the +N ammonium ion group of MG dye adsorption.

The plot of zero-point pH measurement is shown in Fig. 7. The results indicated to negative charge surface of PAN precursor beads and it becomes positively charged below the zero point charge ($\text{pH}_{\text{pzc}} = 7.2$).

3.2. Dye removal dynamic study

3.2.1. Effect of initial pH

The adsorption mechanism is pH-dependent, including pH effects on both adsorbent and adsorbate. The initial pH affects the adsorbent's surface charge and the dissociation of the ions present in the solution. The pH also influences the chemical structure of the dye and thus the color intensity. Therefore, the impact of pH on MG dye has been studied in the range of 3–10. Solutions of 10 mg/L MG dye concentration were prepared at various pH values without adsorbent and left for 2 h. The initial absorbance was measured at 618 nm; then, the absorbance was measured again after 2 h. It was noted that there was no pH effect over the range 4–7. However, the color removal was more than 55% at other values, and the color vanished completely at pH10. The reduction in color caused by pH is attributed to occurring changes in the chemical structure of the dye solution. Mall et al. observed similar pH effects on MG dye [43].

Fig. 8 shows MG response at different pH values, using 10 mg/L dye, 0.4 g precursor beads at $T = 15^\circ\text{C}$, and 200 rpm. The removal percentage at pH 3 was 87% and increased to 97% as the pH value increased to 7. As the results revealed, the removal of dye improved as the pH increased. At lower pH levels, the solution contains positively charged ion H^+ and the dye molecules interact with the adsorption sites. The (pH_{pzc}) value was 7.2, and at a pH value lower than pH_{pzc} , the surface of the adsorbent becomes positively charged, and electrostatic repulsion occurs [47]. Other researchers have reported similar results [44–46]. The maximum adsorption capacity and removal percentage

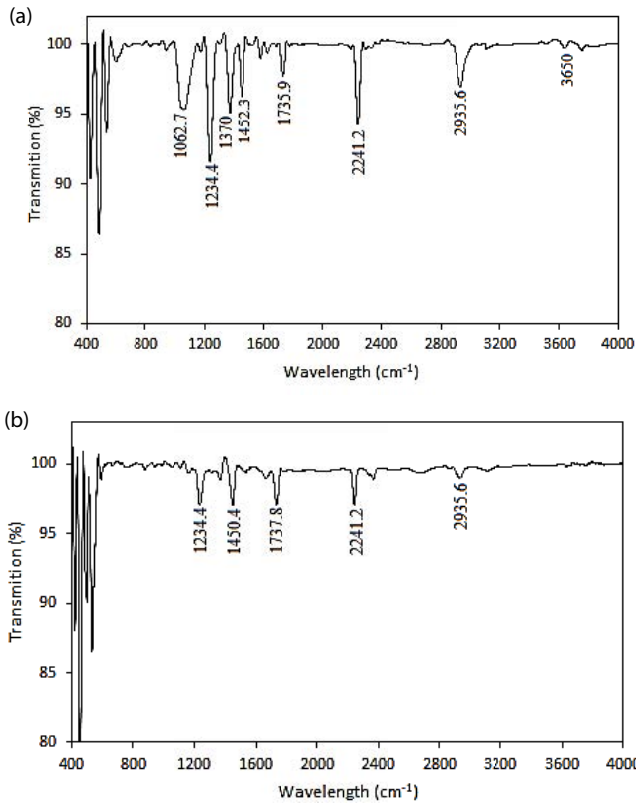


Fig. 6. FTIR spectra of PAN-based precursor beads (a) before and (b) after adsorption.

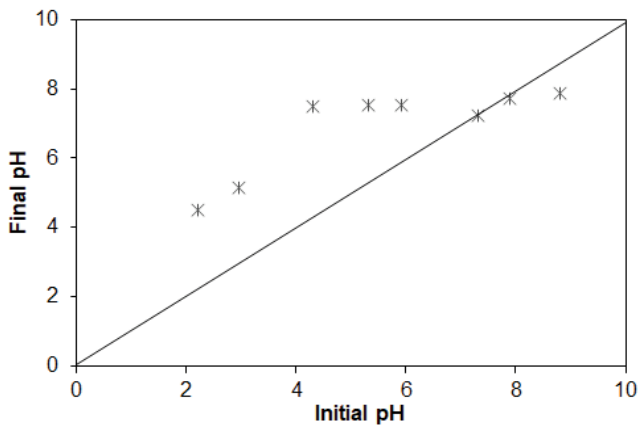


Fig. 7. Point of zero charges (pH_{pzc}) of PAN-based precursor beads.

at pH 7 were 1.369 mg/g and 97%, respectively. As a result, pH 7 was selected as an optimum for the batch experiments.

3.2.2. Effect of mixing rate

Various agitation speeds of 100–300 rpm have been used to detect the effect of the mixing rate on adsorption as shown in Fig. 9. As the rate of mixing increased, the rate of removal percentage increased. At a high agitation rate, the thickness of the boundary layer between the solid and the

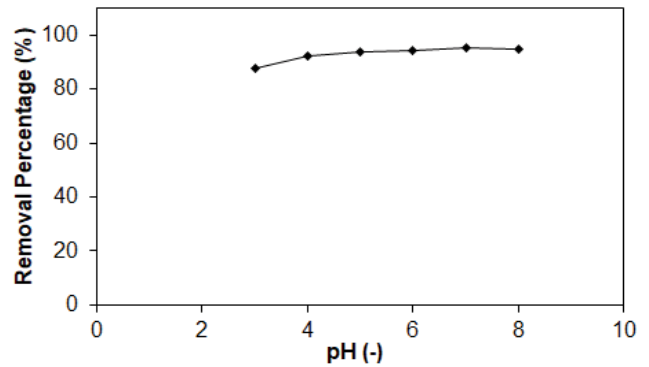


Fig. 8. Effect of pH ($C_0 = 10$ mg/L; 0.4 g beads; 200 rpm; $T = 15^\circ\text{C}$; $t = 5$ h).

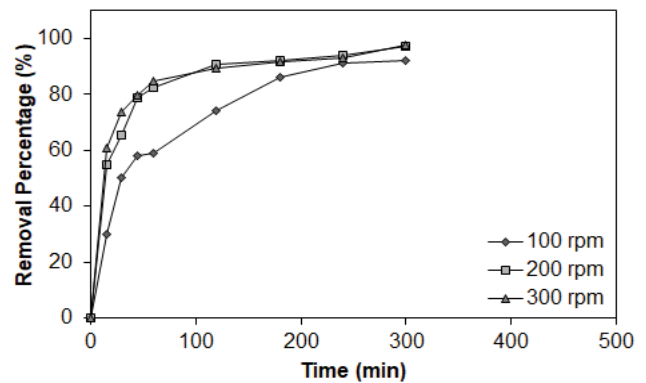


Fig. 9. Effect of agitation speed ($C_0 = 10$ mg/L; 0.4 g beads; pH 7; $T = 15^\circ\text{C}$).

solution is thin. Low resistance to mass transfer and increased the mobility of molecules resulting in rapid removal [48].

3.2.3. Effect of initial dye concentration

Batch experiments with different initial dye concentrations 5–25 mg/L include the removal percentage at pH = 7, 0.4 g adsorbent, 200 rpm, and 15°C are shown in Fig. 10. At the beginning of the MG adsorption process, the percentage removal was rapid then gradually decreased as time progressed to attain equilibrium after 300 min. After 30 min of adsorption and using an initial dye concentration of 10 mg/L, the dye removal percentage was 57% and reached about 96% at equilibrium time. It is also observed that the percentage removal of MG dye decreased from 96% to 78% at equilibrium as initial dye concentration increased to 25 mg/L because the dye molecules compete with each other to reach these sites, thus limiting removal. A similar result had been obtained from other works [49,50]. After 3 h, the removal was 81.45% and 95.44%. After 1 h, the removal slightly increased to 95.5% and 85% for 5 and 25 mg/L initial concentrations, respectively, which is attributed to the reduction in the usable active sites and the electrostatic repulsion between the adsorbent and the bulk solution [51]. On the other hand, the adsorption capacity has increased as the adsorbate has increased. The high

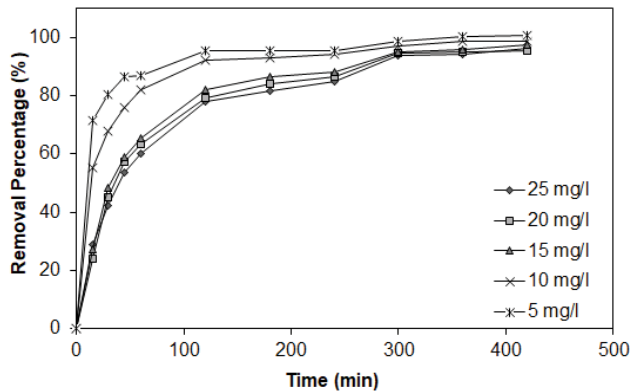


Fig. 10. Effect of contact time at a different initial dye concentration (pH = 7; 0.4 g beads; 200 rpm; $T = 15^\circ\text{C}$).

initial concentration of MG provides the concentration gradient that generates the driving force to overcome the mass transfer resistance between the dye and the adsorbate [2,51].

3.2.4. Effect of adsorbent dose

The effect of various PAN doses 0.2–1 g on the MG dye is shown in Fig. 11. The result revealed that the removal percentage increased as the PAN-based beads dose increased from 0.2 to 1 g. This increase is due to the increase of the surface area resulting in increasing the vacant site up to a specified limit for a fixed number of the dye molecules [21,22]. In contrast, the adsorbed amount per unit mass dropped when the PAN-based beads dose increased. Since the adsorbent dosage is an essential factor that expresses the adsorption capacity at a specific dye concentration, 0.4 g was chosen as the optimum adsorbent dose. The removal percent and the adsorption capacity were 97.13% and 1.457 mg/g, respectively.

3.2.5. Regeneration study

The PAN-based beads were regenerated with 6 M of HCl solution. The regeneration was based on the optimum condition. The used beads were placed in a 50 ml Erlenmeyer flask and agitated at room temperature for 4 h. The beads were then washed with distilled water to remove the excess acid and left to dry at room temperature. Fig. 12 presents a comparison of the pure and regenerated beads. It is observed that a slight reduction in efficiency reached 90% after 2 runs compared to the pure beads 97%. After 5 runs, the removal decreased to 81%; this might be attributed to the active sites are occupied with the MG dye resulting in removal reduction.

3.3. Isotherm study

The adsorption isotherm of any adsorption system is expressed as the curve of the amount of adsorbed molecules on the adsorbent surface. Fig. 13 presents the adsorption capacity and the dye concentration at equilibrium at different temperatures. The most common MG model used to describe the equilibrium adsorption of MG dye is Freundlich and

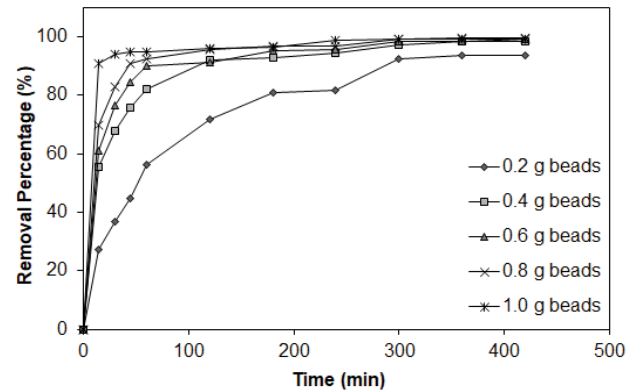


Fig. 11. Effect of PAN-based beads dose ($C_0 = 10 \text{ mg/L}$; pH = 7; 200 rpm; $T = 15^\circ\text{C}$).

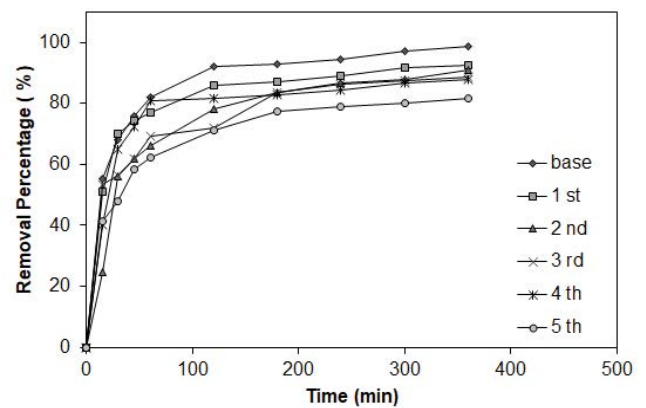


Fig. 12. Adsorbent regeneration ($C_0 = 10 \text{ mg/L}$; 0.4 g beads; pH = 7; 200 rpm; $T = 15^\circ\text{C}$).

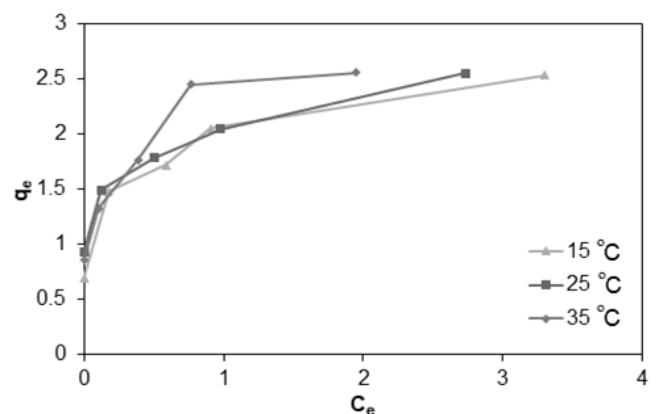


Fig. 13. Adsorption capacity at various temperature.

Langmuir isotherms. The Langmuir isotherm states that all the adsorption sites on the surface of the adsorbent are identical and uniform adsorption energies at the sites. A monolayer of adsorbed molecules covers the adsorbent's surface, and there is no interaction between the adsorbed

molecules on the adsorbent surface. The Langmuir adsorption isotherm can be given by the following equation [52]:

$$\frac{C_e}{q_e} = \frac{1}{K_L \times q_{max}} + \frac{C_e}{q_m} \quad (1)$$

In the equation above C_e (mg/L) and q_m (mg/g) are the concentration of the molecules on the surface at equilibrium and at any time, respectively. q_{max} represents the maximum adsorption capacity (mg/g), and K_L represents the Langmuir constant (L/mg).

The characterization of the Langmuir model can be described by the dimensionless separation factor (R_L): $R_L = 0$ irreversible, $R_L = 1$ linear, $0 < R_L < 1$ favorable, $R_L > 1$ unfavorable [53].

$$R_L = \frac{1}{1 + (K_L \times C_0)} \quad (2)$$

The Freundlich isotherm is an empirical model used to characterize heterogeneous systems. It suggests an interaction between the adsorbed molecules and the non-uniform binding sites of the adsorbent; this model is demonstrated by Eq. (3) [54].

$$\ln q_m = \ln K_F + \frac{1}{n} \times \ln C_e \quad (3)$$

where q_m (mg/g) represents the amount of adsorbed molecules to the adsorbent surface at any time. C_e (mg/L) is the equilibrium concentration. K_F (mg/g) is the Freundlich exponent, which indicates the adsorption capacity. Freundlich constant (n) represents the surface heterogeneity, and high-value (higher than 1) refers to favorable adsorption.

To validate the fitness of the better model, beside the correlation coefficient (R^2), the residual root mean square error (RMSE) value was also evaluated using the following equation [55]:

$$RMSE = \sqrt{\frac{1}{N-1} \sum_{i=1}^m (q_{e,exp} - q_{e,cal})^2} \quad (4)$$

where N represents the number of experimental results. The smaller RMSE and higher R^2 values demonstrate a better model match.

The Langmuir isotherm data are listed in Table 1 and Fig. 14a, while Freundlich isotherm is shown in Table 2

Table 1
Langmuir adsorption isotherm of MG dye at different temperatures

Temp. (K)	R_L	q_m (mg/g)	K_L (L/mg)	R^2	RMSE
288	0.012	2.612	7.979	0.991	0.0412
298	0.010	2.614	7.66	0.989	0.0394
308	0.004	2.617	16.608	0.996	0.0161

RMSE – root mean square error.

and Fig. 14b. The results revealed that the adsorption of MG was suited to the Langmuir isotherm, where the R^2 values are 0.908, 0.982, and 0.994 at 15°C, 25°C, and 35°C, respectively. R_L was between 0 and 1, which revealed that the adsorption process was favorable. The Freundlich exponent (n) with a high value of 8–11 also indicated that the adsorption was favorable. Similar results were reported that the removal of MG dye was fitted to Langmuir isotherm [50,56]. The maximum adsorption capacity obtained was 2.632 mg/g at 15°C.

3.4. Kinetic study

The adsorption takes place in three steps: the transformation of the adsorbate molecular to the adsorbent surface, internal diffusion to the adsorption sites, the surface diffusion. The kinetic study was designed to understand the mechanism of dye adsorption. Two of the most commonly applied kinetics have been used, pseudo-first-order [Eq. (5)] [57] and pseudo-second-order [Eq. (6)] [58].

$$\ln(q_e - q_t) = \ln q_e - \left(\frac{K_1}{2.0303}\right) \times t \quad (5)$$

$$\frac{t}{q_t} = \frac{1}{K_2 \times q_e^2} + \frac{t}{q_e} \quad (6)$$

where q_e is adsorption capacity at equilibrium (mg/g), and q_t is the adsorption capacity at any time (mg/g). The time is t in min while K_1 and K_2 are pseudo-first-order (min^{-1}) and pseudo-second-order (g/mg min).

The values of q_e , K_1 , and K_2 can be identified by plotting $\ln(q_e - q_t)$ vs. t for pseudo-first-order and t/q_t vs. t for pseudo-second-order. The results are shown in Fig. 15, and the estimated values for both models are listed in Table 3.

Pseudo-second-order because R^2 values of the pseudo-second-order model can express the adsorption of MG dye is close to unity. The q values obtained from the pseudo-second-order are much closer to the actual values than pseudo-first-order values. Nethaji et al. [59] has found similar results for MG dye adsorption.

3.5. Thermodynamic study

The thermodynamic parameters, that is, Gibbs free energy change (ΔG°), standard enthalpy change (ΔH°), and standard entropy change (ΔS°), are attributed to the transition mole of solute from the aqueous solution onto the

Table 2
Freundlich adsorption isotherm of MG dye at different temperatures

Temp. (K)	n	K_F (mg/g)	R^2	RMSE
288	8.475	1.992	0.971	0.0326
298	11.236	2.034	0.930	0.0389
308	9.259	2.153	0.873	0.0633

RMSE – root mean square error.

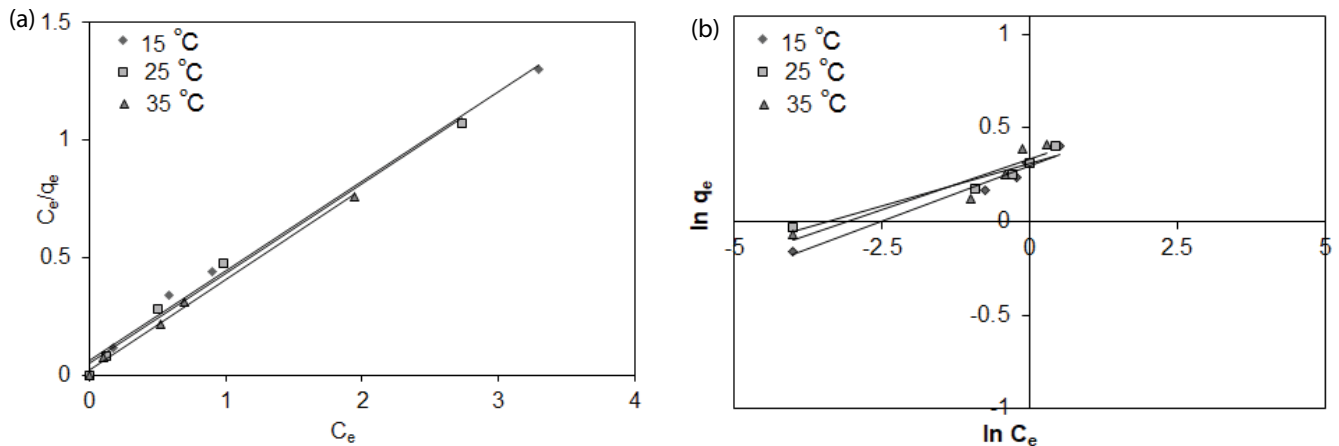


Fig. 14. (a) Langmuir and (b) Freundlich isotherm at different temperatures.

Table 3
Kinetic parameter at different concentrations

Conc. (mg/L)	q_{actual} (mg/g)	Pseudo-first-order				Pseudo-second-order			
		q_{cal} (mg/g)	K_1 (min ⁻¹)	R^2	RMSE	q_{cal} (mg/g)	K_2 (g/mg min)	R^2	RMSE
25	2.535	1.7824	0.0099	0.962	0.0858	2.7196	0.0147	0.9938	2.1296
20	2.051	1.9769	0.0138	0.862	0.2618	2.2075	0.0139	0.9891	3.6299
15	1.722	1.3932	0.0115	0.932	0.1495	1.8349	0.0189	0.9918	3.6142
10	1.479	0.7162	0.0115	0.914	0.1587	1.5083	0.0589	0.9986	1.9471
5	0.694	0.2269	0.0101	0.803	0.2208	0.6774	0.3124	0.9997	2.0886

RMSE – root mean square error.

liquid–solid interface. These parameters are determined to find the effect of temperature on the adsorption process using the following equations:

$$\Delta G = -RT \ln K \quad (7)$$

$$\Delta G = \Delta H - T\Delta S \quad (8)$$

where T and R are the temperature and the ideal gas constant (8.314 J/mol K). While K is the equilibrium constant, that can be expressed by the following equation.

$$K = \frac{C_{\text{Ae}}}{C_{\text{Se}}} \quad (9)$$

where C_{Ae} and C_{Se} are the equilibrium concentration of dye ions on the adsorbent (mg/L) and in the solution (mg/L). The change in standard enthalpy (ΔH°) and change in standard entropy (ΔS°) can be calculated using the Van't Hoff equation by plotting $\ln K$ vs. $1/T$ (Fig. 16). The values of both ΔH° and ΔS° can be obtained from the slope and the intercept, respectively.

$$\ln K = \frac{-\Delta H^\circ}{RT} + \frac{\Delta S^\circ}{R} \quad (10)$$

The results showed a positive value of the enthalpy (16,337.01 J/mol), confirming that the process is endothermic, which means increasing the removal percentage of MG dye with rising the temperature as shown in Fig. 17; a similar result has been found by other researchers [60,61].

The positive value of entropy (74.87 J/mol) suggests that some structural changes might occur due to the interaction between the dye and the fractional group on the beads; it also referred to an increase of randomness in the solid-solution interface [62].

The Arrhenius equation was used to assess the adsorption activation energy, which is defined as the required minimum energy to proceed with the reaction. The activation energy was calculated using the following formula [63]:

$$\ln K_2 = \ln A - \frac{E}{RT} \quad (11)$$

where K_2 and A (g/mol) are pseudo-second-order constant and Arrhenius constant, respectively. The temperature (T) is in K, while R is the gas constant (8.314 J/mol K). The activation energy (E) (kJ/mol) indicates the nature of adsorption and how molecules attach to the adsorbent physically or chemically. Low values (5–40 kJ/mol) refers to physisorption [54], while higher values (40–800 kJ/mol) points to chemisorption [60]. The value of activation energy (23.8445 kJ/mol) is lower than 40 kJ/mol, referring to MG dye's physisorption on PAN precursor beads.

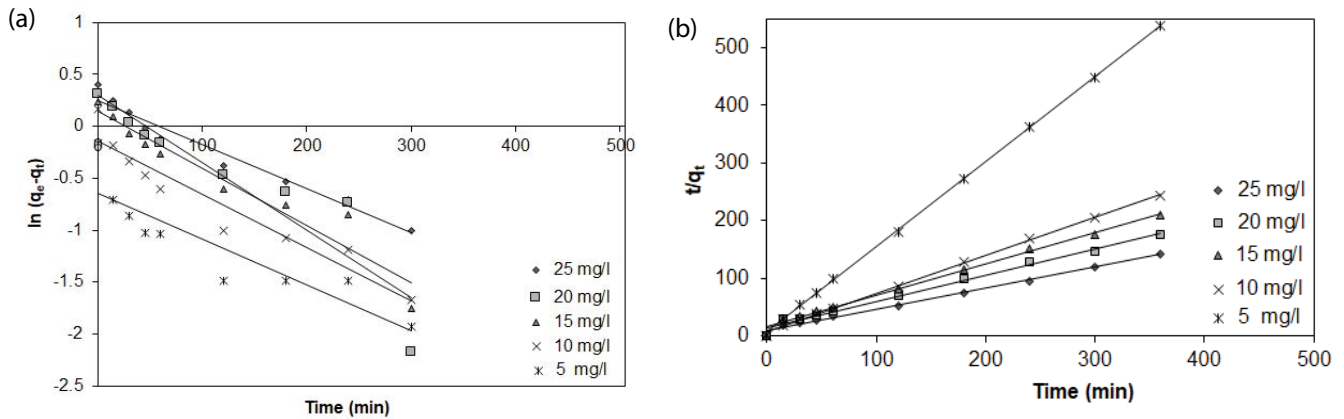


Fig. 15. (a) Pseudo-first-order and (b) pseudo-second-order models at different initial concentrations.

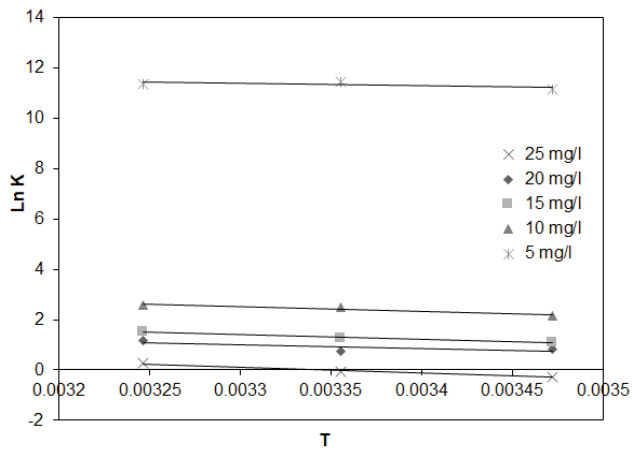


Fig. 16. Van't Hoff plot.

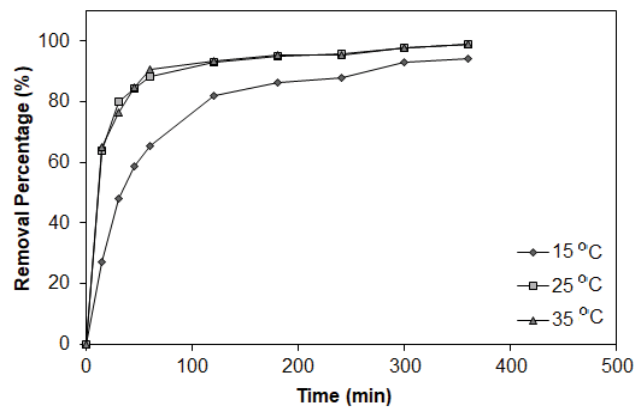


Fig. 17. Temperature effect ($C_0 = 10 \text{ mg/L}$; 0.4 g beads ; $\text{pH} = 7$; 200 rpm).

4. Conclusion

Polyacrylonitrile precursor beads were synthesized using the phase inversion method, and then they were tested to remove MG dye. The specific surface area and average pore diameters were $25 \text{ m}^2/\text{g}$ and 6 nm , respectively.

Different adsorption parameter was studied to conduct its effect on dye removal such as pH, initial dye concentration, PAN dosage, rotating speed, and temperature. The optimum condition were ($\text{pH} = 7$, $C_0 = 10 \text{ mg/L}$, $B_0 = 0.4 \text{ g}$, 200 rpm , $T = 15^\circ\text{C}$) the dye removal and the adsorption capacity were 97% , 2.6315 mg/g , respectively. The adsorbent was regenerated with HCl and tested at the optimum condition. The result showed a slight decrease in the removal up to 5 runs. The dye removal is fitted to Langmuir isotherm. The kinetic study showed that the removal could be expressed by pseudo-second-order. The thermodynamic properties revealed that the process is endothermic and spontaneous.

Acknowledgment

The authors acknowledge the University of Baghdad, chemical engineering, and environmental engineering departments for using their laboratories and equipment to do this research.

References

- [1] E. Eren, O. Cubuk, H. Ciftci, B. Eren, B. Caglar, Adsorption of basic dye from aqueous solutions by modified sepiolite: equilibrium, kinetics and thermodynamics study, *Desalination*, 252 (2010) 88–96.
- [2] R. Ahmad, R. Kumar, Adsorption studies of hazardous malachite green onto treated ginger waste, *J. Environ. Manage.*, 91 (2010) 1032–1038.
- [3] V.K. Garg, R. Kumar, R. Gupta, Removal of malachite green dye from aqueous solution by adsorption using agro-industry waste: a case study of *Prosopis cineraria*, *Dyes Pigment.*, 62 (2004) 1–10.
- [4] V.K. Gupta, S. Khamparia, I. Tyagi, D. Jaspal, A. Malviya, Decolorization of mixture of dyes: a critical review, *Global J. Environ. Sci. Manage.*, 1 (2015) 71–94.
- [5] J.C. Hashimoto, J.A.R. Paschoal, J.F. de Queiroz, F.G.R. Reyes, Considerations on the use of malachite green in aquaculture and analytical aspects of determining the residues in fish: a review, *J. Aquat. Food Prod. Technol.*, 20 (2011) 273–294.
- [6] S.J. Culp, F.A. Beland, Malachite green: a toxicological review, *J. American Coll. Toxicol.*, 15 (1996) 219–238.
- [7] S. Srivastava, R. Sinha, D. Roy, Toxicological effects of malachite green, *Aquat. Toxicol.*, 66 (2004) 319–329.
- [8] M. Kadhom, N. Albayati, H. Alalwan, M. Al-Furajji, Removal of dyes by agricultural waste, *Sustainable Chem. Pharm.*, 16 (2020) 100259, <https://doi.org/10.1016/j.scp.2020.100259>.

- [9] F. Kanwal, R. Rehman, I.Q. Bakhsh, Batch wise sorptive amputation of diamond green dye from aqueous medium by novel Polyaniline-*Alstonia scholaris* leaves composite in ecofriendly way, *J. Cleaner Prod.*, 196 (2018) 350–357.
- [10] R. Rehman, T. Mahmud, M. Irum, Brilliant green dye elimination from water using *Psidium guajava* leaves and *Solanum tuberosum* peels as adsorbents in environmentally benign way, *J. Chem.*, 2015 (2015) 126036, <https://doi.org/10.1155/2015/126036>.
- [11] N.P. Raval, P.U. Shah, N.K. Shah, Malachite green “a cationic dye” and its removal from aqueous solution by adsorption, *Appl. Water Sci.*, 7 (2017) 3407–3445.
- [12] Q. Li, Y.H. Li, X.M. Ma, Q.J. Du, K.Y. Sui, D.C. Wang, C.P. Wang, H.L. Li, Y.Z. Xia, Filtration and adsorption properties of porous calcium alginate membrane for methylene blue removal from water, *Chem. Eng. J.*, 316 (2017) 623–630.
- [13] C. Berberidou, I. Poullos, N.P. Xekoukoulotakis, D. Mantzavinos, Sonolytic, photocatalytic and sonophotocatalytic degradation of malachite green in aqueous solutions, *Appl. Catal., B*, 74 (2007) 63–72.
- [14] J.B. Lee, M.Y. Kim, Photo-degradation of malachite green in mudfish tissues — investigation of UV-induced photo-degradation, *Food Sci. Biotechnol.*, 21 (2012) 519–524.
- [15] L. Ayed, K. Chaieb, A. Cherif, A. Bakhrouf, Biodegradation of triphenylmethane dye malachite green by *Sphingomonas paucimobilis*, *World J. Microbiol. Biotechnol.*, 25 (2009) 705–711.
- [16] N. Daneshvar, M. Ayazloo, A.R. Khataee, M. Pourhassan, Biological decolorization of dye solution containing malachite green by microalgae *Cosmarium* sp., *Bioresour. Technol.*, 98 (2007) 1176–1182.
- [17] A. Mittal, J. Mittal, A. Malviya, D. Kaur, V.K. Gupta, Adsorption of hazardous dye crystal violet from wastewater by waste materials, *J. Colloid Interface Sci.*, 343 (2010) 463–473.
- [18] L.G.T. dos Reis, N.F. Robaina, W.F. Pacheco, R.J. Cassella, Separation of malachite green and Methyl Green cationic dyes from aqueous medium by adsorption on Amberlite XAD-2 and XAD-4 resins using sodium dodecylsulfate as carrier, *Chem. Eng. J.*, 171 (2011) 532–540.
- [19] D. Chen, L. Wang, Y. Ma, W.T. Yang, Super-adsorbent material based on functional polymer particles with a multilevel porous structure, *NPG Asia Mater.*, 8 (2016) e301, <https://doi.org/10.1038/am.2016.117>.
- [20] I. Anastopoulos, I. Pashalidis, A.G. Orfanos, I.D. Manariotis, T. Tatarchuk, L. Sellaoui, A. Bonilla-Petriciolet, A. Mittal, A. Núñez-Delgado, Removal of caffeine, nicotine and amoxicillin from (waste)waters by various adsorbents. A review, *J. Environ. Manage.*, 261 (2020) 110236, doi: 10.1016/j.jenvman.2020.110236.
- [21] R. Malik, D.S. Ramteke, S.R. Wate, Adsorption of malachite green on groundnut shell waste based powdered activated carbon, *Waste Manage.*, 27 (2007) 1129–1138.
- [22] J. Zhang, Y. Li, C.L. Zhang, Y.M. Jing, Adsorption of malachite green from aqueous solution onto carbon prepared from *Arundo donax* root, *J. Hazard. Mater.*, 150 (2008) 774–782.
- [23] B.I. Waisi, S.S. Manickam, N.E. Benes, A. Nijmeijer, J.R. McCutcheon, Activated carbon nanofiber nonwovens: improving strength and surface area by tuning fabrication procedure, *Ind. Eng. Chem. Res.*, 58 (2019) 4084–4089.
- [24] S.K. Sharma, *Green Chemistry for Dyes Removal from Wastewater: Research Trends and Applications*, Scrivener Publishing LLC., 2015.
- [25] A.S. Sartape, A.M. Mandhare, V.V. Jadhav, P.D. Raut, M.A. Anuse, S.S. Kolekar, Removal of malachite green dye from aqueous solution with adsorption technique using *Limonia acidissima* (wood apple) shell as low cost adsorbent, *Arabian J. Chem.*, 10 (2017) S3229–S3238.
- [26] Y. Kismir, A.Z. Aroguz, Adsorption characteristics of the hazardous dye Brilliant Green on Saklikent mud, *Chem. Eng. J.*, 172 (2011) 199–206.
- [27] C. Pradeep Sekhar, S. Kalidhasan, V. Rajesh, N. Rajesh, Bio-polymer adsorbent for the removal of malachite green from aqueous solution, *Chemosphere*, 77 (2009) 842–847.
- [28] G. Crini, Kinetic and equilibrium studies on the removal of cationic dyes from aqueous solution by adsorption onto a cyclodextrin polymer, *Dyes Pigment.*, 77 (2008) 415–426.
- [29] X.B. Luo, Y.C. Zhan, Y.N. Huang, L.X. Yang, X.M. Tu, S.L. Luo, Removal of water-soluble acid dyes from water environment using a novel magnetic molecularly imprinted polymer, *J. Hazard. Mater.*, 187 (2011) 274–282.
- [30] A.A. Elzain, M.R. El-Aassar, F.S. Hashem, F.M. Mohamed, A.S.M. Ali, Removal of methylene dye using composites of poly(styrene-co-acrylonitrile) nanofibers impregnated with adsorbent materials, *J. Mol. Liq.*, 291 (2019) 111335, <https://doi.org/10.1016/j.molliq.2019.111335>.
- [31] R. Rehman, B. Salariya, L. Mitu, Batch scale adsorptive removal of brilliant green dye using trapa natans peels in cost effective manner, *Rev. Chim.*, 67 (2016) 1333–1337.
- [32] O.Y. An, L. Ji, Tailoring the adsorption rate of porous chitosan and chitosan-carbon nanotube core-shell beads, *RSC Adv.*, 4 (2014) 25835–25842.
- [33] K.Y. Foo, B.H. Hameed, Microwave-assisted preparation and adsorption performance of activated carbon from biodiesel industry solid residue: Influence of operational parameters, *Bioresour. Technol.*, 103 (2012) 398–404.
- [34] P. Sukitpaneevit, Y.K. Ong, T.-S. Chung, N. Hilal, PVDF hollow-fiber membrane formation and production, *Membr. Fabr.*, 7 (2015) 215–248.
- [35] S. Rafiei, B. Noroozi, Sh. Arbab, A.K. Haghi, Characteristic assessment of stabilized polyacrylonitrile nanoweb for the production of activated carbon nano-sorbents, *Chin. J. Polym. Sci.*, 32 (2014) 449–457.
- [36] T. Lin, *Nanofibers – Production, Properties and Functional Applications*, Janeza Trdine 9, 51000 Rijeka, Croatia, 2011.
- [37] J.S. Zhuang, M. Li, Y.Q. Pu, A.J. Ragauskas, C.G. Yoo, Observation of potential contaminants in processed biomass using fourier transform infrared spectroscopy, *Appl. Sci.*, 10 (2020) 4345, <https://doi.org/10.3390/app10124345>.
- [38] V. Țucureanu, A. Matei, A.M. Avram, V. Țucureanu, A. Matei, A. Marius, et al., Critical reviews in analytical chemistry FTIR spectroscopy for carbon family study FTIR spectroscopy for carbon family study, *Crit. Rev. Anal. Chem.*, 46 (2016) 502–520.
- [39] B.I. Waisi, Carbonized copolymers nonwoven nanofibers composite: surface morphology and fibers orientation, *Iraqi J. Chem. Pet. Eng.*, 20 (2019) 11–15.
- [40] K. Singh, C. Shah, C. Dwivedi, M. Kumar, P.N. Bajaj, Study of uranium adsorption using amidoximated polyacrylonitrile-encapsulated macroporous beads, *J. Appl. Polym. Sci.*, 127 (2013) 410–419.
- [41] J. Yao, H.J. Ji, H.Z. Lu, T.T. Gao, Effect of tetrahydrofuran extraction on surface functional groups of coking coal and its wettability, *J. Anal. Methods Chem.*, 2019 (2019) 1285462, doi: 10.1155/2019/1285462.
- [42] M. Aliabadi, M. Irani, J. Ismaeili, H. Piri, M. Javad Parnian, Electrospun nanofiber membrane of PEO/Chitosan for the adsorption of nickel, cadmium, lead and copper ions from aqueous solution, *Chem. Eng. J.*, 220 (2013) 237–243.
- [43] I.D. Mall, V.C. Srivastava, N.K. Agarwal, I.M. Mishra, Adsorptive removal of malachite green dye from aqueous solution by bagasse fly ash and activated carbon-kinetic study and equilibrium isotherm analyses, *Colloids Surf., A*, 264 (2005) 17–28.
- [44] M. Ghaedi, A. Ansari, M.H. Habibi, A.R. Asghari, Removal of malachite green from aqueous solution by zinc oxide nanoparticle loaded on activated carbon: kinetics and isotherm study, *J. Ind. Eng. Chem.*, 20 (2014) 17–28.
- [45] M.A. Ahmad, R. Alrozi, Removal of malachite green dye from aqueous solution using rambutan peel-based activated carbon: equilibrium, kinetic and thermodynamic studies, *Chem. Eng. J.*, 171 (2011) 510–516.
- [46] B.H. Hameed, M.I. El-Khaiary, Batch removal of malachite green from aqueous solutions by adsorption on oil palm trunk fibre: equilibrium isotherms and kinetic studies, *J. Hazard. Mater.*, 154 (2008) 237–244.

- [47] Z. Harrache, M. Abbas, T. Aksil, M. Trari, Thermodynamic and kinetics studies on adsorption of Indigo Carmine from aqueous solution by activated carbon, *Microchem. J.*, 144 (2019) 180–189.
- [48] B.K. Nandi, A. Goswami, M.K. Purkait, Adsorption characteristics of brilliant green dye on kaolin, *J. Hazard. Mater.*, 161 (2009) 387–395.
- [49] M. Saif Ur Rehman, M. Munir, M. Ashfaq, N. Rashid, M.F. Nazar, M. Danish, J.-I. Han, Adsorption of Brilliant Green dye from aqueous solution onto red clay, *Chem. Eng. J.*, 228 (2013) 54–62.
- [50] S.D. Khattri, M.K. Singh, Removal of malachite green from dye wastewater using neem sawdust by adsorption, *J. Hazard. Mater.*, 167 (2009) 1089–1094.
- [51] Y.Y. Yao, H. Bing, X. Feifei, C. Xiaofeng, Equilibrium and kinetic studies of methyl orange adsorption on multiwalled carbon nanotubes, *Chem. Eng. J.*, 170 (2011) 82–89.
- [52] F. Jiang, D.M. Dinh, Y.-L. Hsieh, Adsorption and desorption of cationic malachite green dye on cellulose nanofibril aerogels, *Carbohydr. Polym.*, 173 (2017) 286–294.
- [53] K.R. Hall, L.C. Eagleton, A. Acrivos, T. Vermeulen, Pore- and solid-diffusion kinetics in fixed-bed adsorption under constant-pattern conditions, *Ind. Eng. Chem. Fundam.*, 5 (1966) 212–223.
- [54] T.A. Saleh, A.A. Al-Absi, Kinetics, isotherms and thermodynamic evaluation of amine functionalized magnetic carbon for methyl red removal from aqueous solutions, *J. Mol. Liq.*, 248 (2017) 577–585.
- [55] R. Saadi, Z. Saadi, R. Fazaeli, N.E. Fard, Monolayer and multilayer adsorption isotherm models for sorption from aqueous media, *Korean J. Chem. Eng.*, 32 (2015) 787–799.
- [56] Y. Önal, C. Akmil-Başar, Ç. Sarıçı-Özdemir, Investigation kinetics mechanisms of adsorption malachite green onto activated carbon, *J. Hazard. Mater.*, 146 (2007) 194–203.
- [57] G.S. Gupta, G. Prasad, V.N. Singh, Removal of chrome dye from aqueous solutions by mixed adsorbents: fly ash and coal, *Water Res.*, 24 (1990) 45–50.
- [58] D. Robati, M. Rajabi, O. Moradi, F. Najafi, I. Tyagi, S. Agarwal, V.K. Gupta, Kinetics and thermodynamics of malachite green dye adsorption from aqueous solutions on graphene oxide and reduced graphene oxide, *J. Mol. Liq.*, 214 (2016) 259–263.
- [59] S. Nethaji, A. Sivasamy, G. Thennarasu, S. Saravanan, Adsorption of malachite green dye onto activated carbon derived from *Borassus aethiopum* flower biomass, *J. Hazard. Mater.*, 181 (2010) 271–280.
- [60] M.-H. Baek, C.O. Ijagbemi, S.-J. O, D.-S. Kim, Removal of malachite green from aqueous solution using degreased coffee bean, *J. Hazard. Mater.*, 176 (2010) 820–828.
- [61] Y. Önal, C. Akmil-Başar, Ç. Sarıçı-Özdemir, Investigation kinetics mechanisms of adsorption malachite green onto activated carbon, *J. Hazard. Mater.*, 146 (2007) 194–203.
- [62] A.A. Jalil, S. Triwahyono, S.H. Adam, N.D. Rahim, M.A.A. Aziz, N.H.H. Hairom, N.A.M. Razali, M.A.Z. Abidin, M.K.A. Mohamadiah, Adsorption of methyl orange from aqueous solution onto calcined Lapindo volcanic mud, *J. Hazard. Mater.*, 181 (2010) 755–762.
- [63] A.A. El-Bindary, M.A. Hussien, M.A. Diab, A.M. Eessa, Adsorption of Acid Yellow 99 by polyacrylonitrile/activated carbon composite: kinetics, thermodynamics and isotherm studies, *J. Mol. Liq.*, 197 (2014) 236–242.